Applicability of Large-Scale Convection and Condensation Parameterization to Meso-γ-Scale HIRLAM: A Case Study of a Convective Event

SAMI NIEMELÄ AND CARL FORTELIUS

Finnish Meteorological Institute, Helsinki, Finland

(Manuscript received 17 August 2004, in final form 8 February 2005)

ABSTRACT

This paper presents a case study of a single cold air outbreak event with widespread convective precipitation over southern Finland on 25 May 2001. The purpose of the study is to investigate the applicability of the convection and condensation scheme of the High-Resolution Limited Area Model (HIRLAM) on meso-γ-scales. The study concentrates on the issue of grid-size-dependent convection parameterization. An explicit approach without the convection scheme is also examined. At the same time, the performance of an experimental nonhydrostatic version of HIRLAM is evaluated. Model simulations are conducted with three different horizontal grid spacings: 11, 5.6, and 2.8 km. Model results are compared to observed radar reflectivity data utilizing a radar simulation model, which calculates radar reflectivities from three-dimensional model output.

The best results are obtained using nonhydrostatic dynamics and a grid-size-dependent convection scheme with a 5.6-km grid interval. However, even the best configuration still overestimates the area of strong reflectivity (intense precipitation). All the other combinations produce even stronger reflectivity. The grid-size-dependent convection parameterization is evidently beneficial at smaller grid spacings than 5.6 km. The nonhydrostatic model clearly outperforms its hydrostatic counterpart at the 5.6- and 2.8-km grid spacings, whereas with an 11-km grid interval, both models perform equally well.

1. Introduction

There is a growing need for improvement of precipitation forecasts. The intensity of strong convective rain events in particular is not adequately covered by large-scale models. Accordingly, the development of meso-γ-scale (2–20 km, after Orlanski 1975) numerical weather prediction (NWP) models is a very topical issue. These models cannot resolve individual convective elements, but they can resolve organized mesoscale convective systems or squall lines. Precipitation forecasts are very important for hydrological applications. Catchment models can employ such forecasts in real-time prediction of river flows (Montanari and Uhlenbrook 2004) and flood events. Hydrological models are also essential tools for planning the optimal management of water resources (Uhlenbrook et al. 2004). In addition, precipitation intensity is a critical parameter for air quality and dispersion modelers in estimation of the scavenging effects of air pollutants, as described in the classical work by Chamberlain (1953).

The representation of convective phenomena is very difficult in meso-γ-scale models. The rapid development of computing power has enabled limited area NWP models to use a grid spacing of about 10 km. Weisman et al. (1997) proposed that organized convective structures could be resolved explicitly with a smaller grid spacing than 4 km. However, Molinari and Dudek (1992) argued that with such scales, the use of explicit methods only moves the parameterization issues into the turbulence and microphysical schemes. A consensus prevails in the scientific community that a sophisticated microphysical treatment, with prognostic variables for precipitating hydrometeors, should be used for such resolutions (e.g., Tao et al. 2003).

According to Molinari and Dudek (1992), the grid spacing range of 5–20 km is especially difficult for convection schemes to handle. Several studies have shown that some parameterization is still needed, because the explicit simulation of convection produces slowly evolving and overshooting precipitation events (e.g., Zhang et al. 1988; Wang and Seaman 1997; Bélair and Mailhot

Corresponding author address: Sami Niemelä, Finnish Meteorological Institute, P.O. Box 503, FI-00101 Helsinki, Finland.
E-mail: sami.niemela@fmi.fi

2001; Liu et al. 2001). Molinari and Dudek (1992) also pointed out that successful simulation with the explicit approach is very case dependent; there should be strong grid-scale forcing and weak convective instability.

Jung and Arakawa (2004) showed that convection parameterization is highly dependent on the model resolution (in both time and space) in the range of meso-γ-scales. Traditionally, convection parameterizations are "tuned" for a fixed grid spacing. Therefore, the behavior of nonresolution-dependent convection schemes may be undesirable, when these schemes are applied for different scales. Jung and Arakawa (2004) and Arakawa (2004) argued that the formulations of future physical parameterizations should include resolution dependencies.

Explicit treatment of convection (2–3-km scale) with sophisticated microphysical parameterization is still computationally extremely expensive. Consequently, the transition from scales used in current operational models (about 10–20 km) to kilometer scale will take years. Still the urgent need for better precipitation forecasts remains. Weather services that lack high computing power would especially benefit if a computationally more efficient "intermediate" solution could be found.

The objective of this study is to evaluate the applicability of the existing convection and condensation scheme (originally designed for meso-β-scales) of the High Resolution Limited Area Model (HIRLAM) in meso-γ-scale convective conditions. Hammarstrand (1998) showed that HIRLAM's convection scheme is able to produce better precipitation forecasts with a 22-km grid spacing as compared to 55 km. However, the resolution dependency issues were not studied. Here, special emphasis is given to a comparison of both simple grid-size-dependent and nonresolution-dependent convection schemes.

Kato and Saito (1995) showed that the hydrostatic assumption is no longer valid in moist convective conditions for scales of less than 10 km. Therefore, the performance of a nonhydrostatic version of the model is also examined. We especially concentrate on finding a grid-size range where the hydrostatic and nonhydrostatic models start to perform differently. For these reasons, a case study of a single cold air outbreak event over Southern Finland is conducted. The performance of the different model configurations is mainly validated using radar reflectivity data from the Finnish radar network. Modeled radar reflectivities are produced by using the Radar Simulation Model (RSM) of Haase and Crewell (2000).

2. Description of the model

HIRLAM is a complete NWP system including a hydrostatic primitive equation model with an extensive set of physical parameterizations and data assimilation. The multilayer primitive equations have been discretized using a hybrid (η) coordinate system in the vertical. A more detailed description of the whole HIRLAM system is given in Undén et al. (2002). The present study is based on HIRLAM version 6.1.0 including the following physical parameterization schemes.

a. Physical parameterizations

The turbulence scheme is based on prognostic turbulent kinetic energy (TKE) and a diagnostic length scale. This TKE-*l* scheme is adapted from the planetary boundary layer model by Cuxart et al. (2000). Soil and surface processes are modeled using the Interaction Soil–Biosphere–Atmosphere (ISBA) scheme (Noilhan and Planton 1989). In the current implementation, three land surface types and two soil layers are available. Soil temperature and water content are dealt with utilizing force–restore methods. The fast radiation code is based on the work of Savijärvi (1990).

The Soft Transition Condensation (STRACO; Sass 2002) parameterizes both convective and stratiform condensation, clouds, and precipitation. It also allows a gradual transition between both regimes. The actual transition is handled by relaxing the fractional cloud cover toward equilibrium, in which the cloud may be either in the convective or stratiform state, depending on the case. STRACO was originally developed for use on meso-β-scales. However, an improved applicability for meso-γ-scales is sought by introducing simple grid-size-dependent functions in the convective part of the scheme.

The STRACO scheme acts on the temperature T, specific humidity q, and combined cloud water and ice content q_c. It uses also the horizontal wind components u and v and the surface pressure p_s. The scheme follows closely the work by Sundqvist et al. (1989) and Sundqvist (1993). The convective part is based on a moisture accession closure, as does the well-known Kuo (1974) scheme. However, the STRACO scheme differs considerably from the original Kuo scheme. The present version of the cumulus parameterization does not directly produce any precipitation. Moreover, the scheme increases q_c, which is a grid-scale prognostic variable. The precipitation release depends on q_c.

The triggering mechanism for convection defines convective air columns by lifting air layers. A convectively active column is obtained if a lifted air layer ex-

periences positive buoyancy. The lifting method depends explicitly on the horizontal grid spacing in two ways. Firstly, a resolution-dependent perturbation temperature

$$\Delta T_{\text{per}} = \left(0.6\ \text{K}^{-1} + 0.5\ \text{K}^{-1} \sqrt{\frac{10\ \text{km}}{D}} \right)^{-1}, \quad (1)$$

and specific humidity

$$\Delta q_{\text{per}} = 0.02\ q_k \sqrt{\frac{D}{10\ \text{km}}}, \quad (2)$$

are used at the beginning of the lifting process, so that the convective condition becomes easier to satisfy as the grid spacing increases. Here D is the grid spacing (km) and q_k is the specific humidity at the bottom of the convective air column considered. Second, the cloudy air (T_c and q_s) is mixed with cooler ambient air (T and q) during the air parcel ascent,

$$T_{\text{mix}} = (1 - \epsilon_e)T_c + \epsilon_e T, \quad (3)$$

$$q_{\text{mix}} = (1 - \epsilon_e)q_s + \epsilon_e q, \quad (4)$$

by using a grid-size-dependent entrainment function,

$$\epsilon_e = \left(1.3 \times 10^{-4}\ \text{m}^{-1} + \frac{7.5 \times 10^{-4}\ \text{m}^{-1}}{\text{Ri}_*} \right) \times \left(\frac{z}{500\ \text{m} + z} \right) \left(\frac{10\ \text{km}}{D} \right), \quad (5)$$

where z is height (m) and

$$\text{Ri}_* = \left(1.0 \times 10^{-4}\ \text{km}^{-1} + \left| \frac{\partial \theta}{\partial z} \right| \right) \left(\frac{\theta}{g} \left| \frac{\partial V}{\partial z} \right|^2 \right)^{-1} \quad (6)$$

is a Richardson number. In Eq. (6) θ is the potential temperature, g is gravity, and V is the horizontal wind speed. The first two terms in Eq. (5) together ensure that the maximum entrainment is obtained near the cloud base, as described by Cohen (2000). Equation (5) states that lateral mixing will restrict the formation of convective entities by decreasing the buoyancy as the grid spacing reduces, the height increases and the wind shear strengthens (through Ri_*). Thus, Eq. (5) gradually switches the convection parameterization off by restricting the depth of the convective cloud [see Eqs. (7)–(9) and (14) below] as the grid spacing decreases.

In the STRACO scheme, the basic equations for T, q, and q_c are

$$\frac{\partial T}{\partial t} = A_T + \frac{L'}{c_p} \left[\langle Q_a \rangle (1 - \beta) \frac{F_h}{\langle F_h \rangle} \delta_* - E \right] - \frac{L'}{c_p} E_p + S_T, \quad (7)$$

$$\frac{\partial q}{\partial t} = A_q (1 - \delta_*) + \langle Q_a \rangle \beta \frac{F_q}{\langle F_q \rangle} \delta_* + E + E_p + S_q, \quad (8)$$

$$\frac{\partial q_c}{\partial t} = A_{qc} + \langle Q_a \rangle (1 - \beta) \frac{F_c}{\langle F_c \rangle} \delta_* - E - G_p + S_c. \quad (9)$$

On the left-hand side are the combined tendencies of dynamics, radiation, turbulence, and convection, whereas the A terms on the right-hand side represent the tendencies without convection.

The terms including $\langle Q_a \rangle$ represent the convective source terms of temperature, moisture, and cloud water. Here $\langle Q_a \rangle$ is the total moisture input (from the dynamics and turbulence scheme during a physics time step) of the convective cloud per unit time. The vertical averaging operator within the convective cloud is defined as

$$\langle\ \rangle = \frac{1}{p_t - p_b} \int_{p_b}^{p_t} dp, \quad (10)$$

where p_b and p_t are the pressures at the cloud base and top, respectively. Functions describing the vertical variation of convective heating, moistening, and condensation are defined as

$$F_h = T_{\upsilon c} - T_\upsilon, \quad (11)$$

$$F_q = q_{\text{sc}} - q, \quad (12)$$

$$F_c = q_{\text{cc}}, \quad (13)$$

respectively. Index υ means virtual, c stands for the in-cloud value, and s means the saturation value. Here L' and c_p are the specific latent heat of condensation/sublimation and the specific heat capacity at constant pressure. The semiempirical parameter

$$\delta_* = \frac{\Delta p_c}{2 \times 10^4\ \text{Pa}}, \quad (14)$$

where Δp_c is the depth of the convective cloud considered, ensures that only deep convective clouds are fully parameterized. Shallow phenomena ($\delta_* \to 0$) are left for the turbulence scheme to handle. The variable δ_* is constrained never to exceed unity.

The moistening parameter β is used to determine the partitioning of moisture input between moistening [Eq. (8)] and heating/cloud condensate [Eqs. (7) and (9)]. Two alternative approaches for β are considered. The first is a function of the relative humidity RH:

$$\beta = (1 - \langle \text{RH} \rangle)^2, \quad (15)$$

which is similar to that originally described by Anthes (1977). In moist conditions (small β) the moisture input is mainly transferred to convective heating and condensation, whereas in dry conditions (large β) the convec-

tion scheme moistens the air column. The second approach is based on a grid-size-dependent formulation (B. H. Sass 2004, personal communication):

$$\beta = \frac{1}{\left(1 + \frac{D}{3\ \text{km}}\right)}. \tag{16}$$

Observational studies of Braham (1952) indicate that more than 50% of the water vapor inflow to small thunderstorms is condensed into cloud. If the grid size is larger than 3 km, small-scale thunderstorms still need to be parameterized. Therefore, Eq. (16) ensures that most of the moisture input (more than 50%) is directed to increase the prognostic cloud condensate. If the grid size is smaller than 3 km, it may be possible to represent the thunderstorms on a resolvable scale. However, the purpose of β is not to switch off parameterized convection. This decision is made during the triggering phase [Eq. (5)].

The terms including $\langle Q_a \rangle$ and β in Eqs. (7)–(9) are only active in convective air columns. All the other terms are employed in both convective and stratiform regimes. Moistening and heating can also occur from the evaporation of cloud condensate E and precipitation E_p. The S terms represent the heat and moisture fluxes through the interface between a convective cloud and the stable atmosphere above. A detailed description of these terms is presented by Sass (2002).

Finally, the diagnostic rate of precipitation release G_p is based on the formulation by Sundqvist et al. (1989):

$$G_p = \Phi q_c \left[1 - \exp\left(-\frac{q_c}{b\mu}\right)\right], \tag{17}$$

where Φ^{-1} is a characteristic time for the conversion of cloud drops to rain drops, μ is the threshold value for cloud water, and b is the fractional cloud cover. The difference between convective and stratiform regimes is introduced by utilizing different constants as described below. The formulation of the conversion coefficient is

$$\Phi = [\phi + K_\Phi \omega_* (\phi - \phi_0)](\Phi_{\text{co}} + \Phi_{\text{bf}}) \tag{18}$$

$$\omega_* = \begin{cases} 0 & \text{if} \quad \omega > 0 \\ \omega & \text{if} \quad \omega \le 0 \end{cases},$$

where ω is the vertical velocity in pressure coordinates, Φ_{co} is a function to represent the coalescence processes, and Φ_{bf} is a function to simulate the enhanced precipitation release when ice crystals coexist with water droplets (the Bergeron–Findeisen effect). More detailed information about the above functions is given by Sass (2002). The values of coefficients ϕ, ϕ_0, and K_Φ are given in Table 1. The threshold value for cloud water is

TABLE 1. Coefficients related to precipitation release in the convective and stratiform regimes [Eqs. (17)–(19)]. Here $B = (T_{vc} - T_v)/T_v$ is buoyancy and $|K_\mu|$ is restricted to be no larger than 1.

Coefficient	Convective regime	Stratiform regime
ϕ (s^{-1})	2.5×10^{-4}	1.0×10^{-4}
ϕ_0 (s^{-1})	1.0×10^{-5}	1.0×10^{-5}
K_Φ (Pa^{-1} s)	2.0×10^{-2}	2.0×10^{-2}
μ_0 (kg kg^{-1})	5.0×10^{-4}	5.0×10^{-4}
μ_1 (kg kg^{-1})	3.0×10^{-3}	5.0×10^{-4}
μ_2 (kg kg^{-1})	5.0×10^{-4}	3.0×10^{-3}
K_μ	$-K_\Phi \omega_* + 250B$	$K_\Phi \omega_*$

$$\mu = \frac{[\mu_0 + K_\mu(\mu_1 - \mu_2)]}{\Phi_{\text{co}} + \Phi_{\text{bf}}}. \tag{19}$$

The coefficients μ_0, μ_1, μ_2, and K_μ for the stratiform and convection regimes are also given in Table 1. With negligible vertical velocity, the formation of precipitation is more efficient in the convective regime (cr) compared to the stratiform regime (sr) [$\Phi_{\text{cr}} > \Phi_{\text{sr}}$ in Eq. (17)]. However, a model-resolved updraft tends to suppress the precipitation release by decreasing Φ and increasing μ. This simulates the delaying effect of precipitation onset by vertically advected hydrometeors. The effect will become important at high model resolutions, since larger vertical velocities will be simulated.

b. Nonhydrostatic dynamics

An anelastic pressure-coordinate-based nonhydrostatic version of HIRLAM has been developed by Rõõm (2001) and Männik and Rõõm (2001). In the anelastic approximation, all internal acoustic wave modes are filtered and large time steps are allowed, even with an explicit time scheme. The external (Lamb) mode is filtered using a surface pressure adjustment. Männik et al. (2003) proved that this anelastic approach was able to produce as good results as its hydrostatic counterpart with an 11-km grid spacing. However, it is still unproven that this nonhydrostatic model performs better than a hydrostatic model in a real case with a smaller grid spacing.

c. The RSM

Meteorological radars generally transmit short pulses of electromagnetic radiation from a directional antenna, and register the power reflected by hydrometeors (cloud droplets, ice crystals, raindrops, snowflakes, hail, etc.) and other objects. The amplitude of the returned signal is used to estimate the reflectance factor

TABLE 2. Summary of the conducted experiments.

Name	Dynamics	Convection scheme: Triggering [Eqs. (1), (2), and (5)]	Convection scheme: β parameter
HH-1	Hydrostatic	$\propto D$	Eq. (16) $\propto D$
NHH-1	Nonhydrostatic	$\propto D$	Eq. (16) $\propto D$
NHH-2	Nonhydrostatic	$\propto D$	Eq. (15) $\propto \langle RH \rangle$
NHH-3	Nonhydrostatic	No D dependency*	Eq. (15) $\propto \langle RH \rangle$
NHH-NC	Nonhydrostatic	No convection scheme	

* The square root terms of Eqs. (1)–(2) and the third term on the right-hand side of Eq. (5) are equal to 1.

or reflectivity of the target volume. The reflectivity depends on the amount and phase of the hydrometeors, and on the particle size distribution. The RSM (Haase and Crewell 2000) is a software package that simulates radar measurements corresponding to the output of a NWP model (Haase and Fortelius 2001). The assumed location, frequency, and scan pattern can all be chosen to match any available radar data within the model domain. RSM then computes the local reflectivity at each grid point of the model, and generates a simulated measurement by taking into account the beam propagation and attenuation within the simulated atmosphere.

The purpose of RSM is to make it possible to use radar measurements for forecast verification directly, without having to solve the difficult problem of linking the observed reflectivity to precipitation at the ground.

3. Experimental setup

To achieve the objectives of the study, 15 different model simulations of a single cold air outbreak event with convective precipitation are carried out. The event occurred over southern Finland on 25 May 2001. During that day, a stationary low pressure system was located east of Finland, giving rise to northerly winds. This cold airflow aloft over a diurnally heated surface during a clear morning created favorable conditions for convective instability to build up. At 0900 LT (= UTC + 3 h) the first convective precipitation cells were observed. At 1300 LT almost the whole of southern Finland was covered with small-scale, shallow cells with little mesoscale organization. The event gradually disappeared between 1300 and 2200 LT. These kinds of convective conditions are common in Finland during May and early June.

Table 2 summarizes five basic experiments with variable model configurations. The differences in the performance of hydrostatic and nonhydrostatic models can be studied by comparing the hydrostatic (HH-1) and nonhydrostatic (NHH-1) experiments. The comparison between NHH-1 and NHH-2 focuses on the choice of the β parameter. Issues concerning the grid-size dependency of the convection scheme are studied by comparing NHH-1, NHH-2, and NHH-3.

Each experiment was carried out by utilizing three different horizontal grid spacings: 11, 5.6, and 2.8 km. The integration domain for the coarse grid experiments covers almost the whole of Scandinavia, whereas the domain with the most dense grid includes only southern Finland and the Gulf of Finland (see Fig. 1). Each domain has 156×156 horizontal grid points with 40 vertical levels. The grid interval in the vertical increases with height. For the lowest 1 km the vertical grid interval varies between 70 and 200 m. The lowest η level is at about 30 m. For all the experiments, analyses from the operational HIRLAM runs of the Finnish Meteorological Institute (22-km grid spacing) are used as boundaries. Each experiment includes a semi-implicit Eulerian time integration scheme and its own data assimilation step, whereby the initial state is determined by statistical interpolation methods. The time steps for grid spacings of 11, 5.6, and 2.8 km are 60, 30, and 10 s, respectively. The integration time is 21 h starting at 0000 UTC 25 May 2001.

4. Results

All the results are examined within the area covered by three radars: Anjalankoski (60.9°N, 27.1°E), Ikaalinen (61.8°N, 23.1°E), and Vantaa (60.3°N, 24.9°E). This area is approximately the same as the smallest calculation area with a 2.8-km horizontal grid spacing. We do not expect to correctly predict the position of individual convective cells. Rather, we concentrate on the overall coverage of the precipitation areas, reflectivity distributions, and areally averaged precipitation amounts.

Figure 1 shows the radar reflectivity fields from the experiments with the highest model resolution after 12 h of simulation. It can be seen from the observed field (Fig. 1f) that almost the whole of southern Finland was covered by small-scale convection. All models are able to form cellular structures similar to the observed ones (width of cells 8–10 grid points). However, it is clearly seen that even a 2.8-km grid spacing is not fine enough to describe such small-scale features. The total area of precipitation is well represented by all experiments except the hydrostatic one (HH-1), which creates only a few strong precipitation cells.

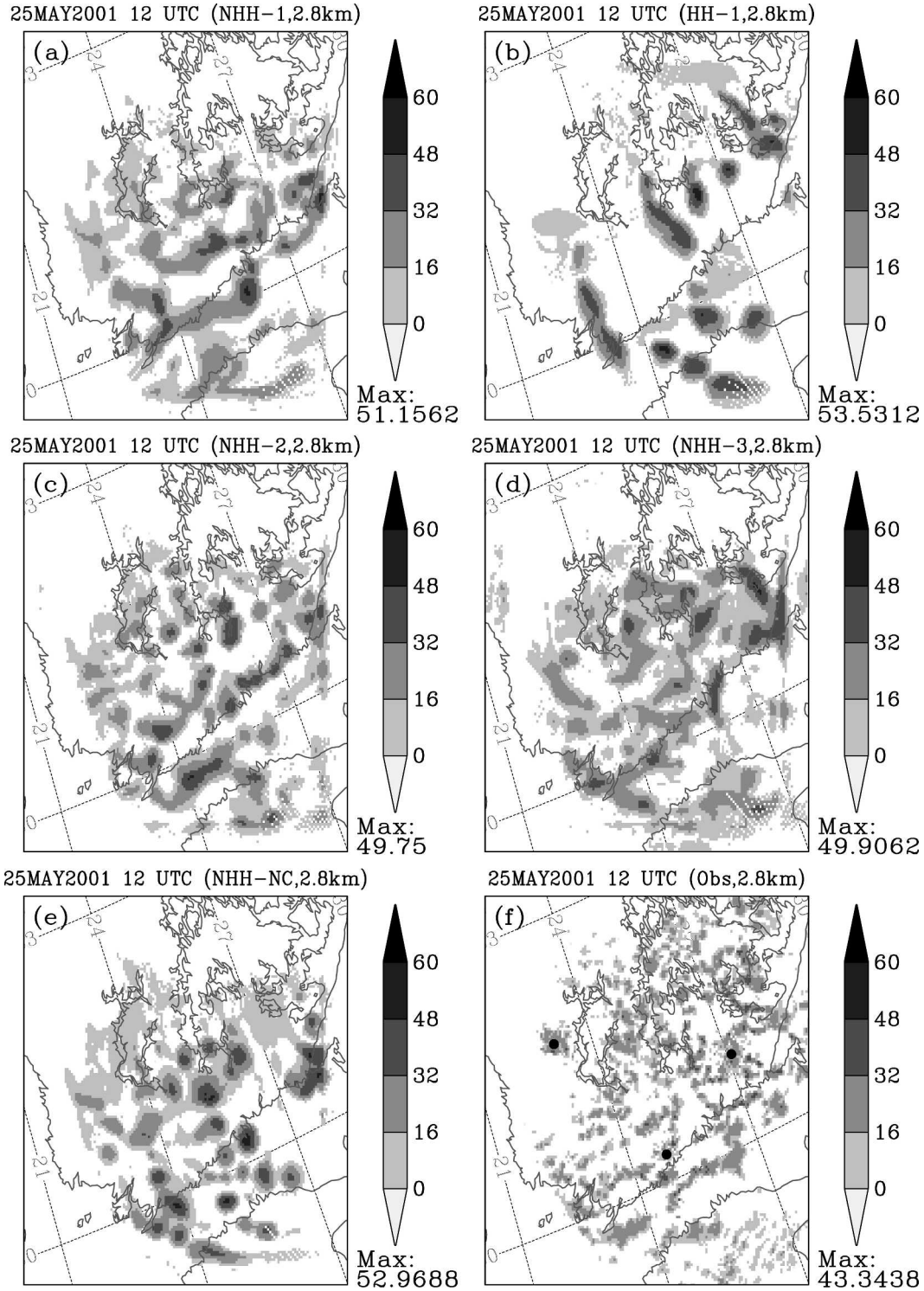

FIG. 1. Composite radar reflectivity (dBZ) fields after a 12-h simulation valid at 1200 UTC 25 May 2001: (a) NHH-1, (b) HH-1, (c) NHH-2, (d) NHH-3, (e) NHH-NC, and (f) radar observation. The horizontal grid spacing of each field is 2.8 km. The maximum dBZ value within the area is given next to each panel. The locations of the radars are marked with dots in (f).

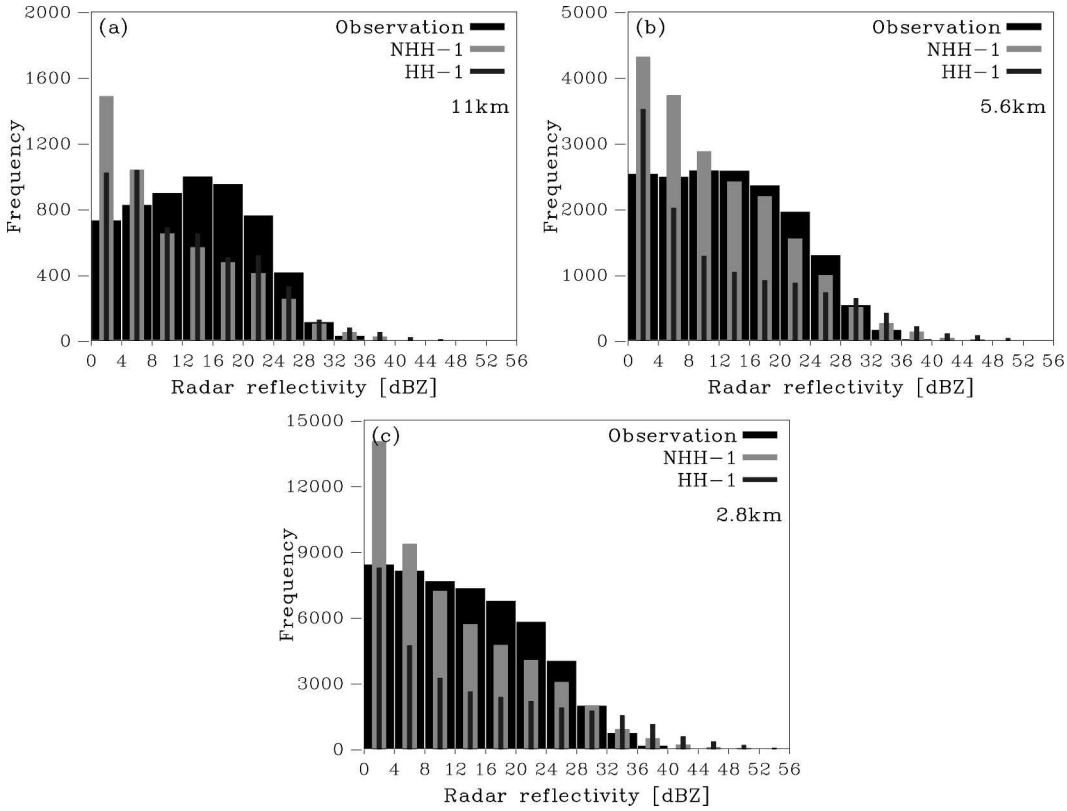

FIG. 2. Frequency distributions of radar reflectivity (dBZ) produced by 21-h simulations (NHH-1 and HH-1) starting at 0000 UTC 25 May 2001. Horizontal grid spacings are (a) 11, (b) 5.6, and (c) 2.8 km. Black bars represent dBZ observations. The radar antenna elevation is 0.4°. In this case, reflectivity values below 0 dBZ are not meteorologically important and are therefore omitted.

a. Comparison between hydrostatic and nonhydrostatic models

The radar reflectivity distributions of HH-1 and NHH-1 experiments are compared in Fig. 2. Overall the best frequency distribution is produced by the NHH-1 with a 5.6-km grid spacing. With an 11-km grid spacing, the behavior of both models is very similar. However, with grid spacings of 5.6 and 2.8 km, HH-1 overestimates the amount of strong reflectivity values (>32 dBZ) more than NHH-1. On the other hand, the number of moderate reflectivity values (8–32 dBZ) is severely underestimated in HH-1, whereas NHH-1 performs very well. With the highest model resolution, HH-1 tends to form only a few precipitation cells having a very strong intensity (cf. Fig. 1b).

The nonhydrostatic model performs somewhat better than the hydrostatic model, regardless of the choice for the convection scheme configuration. The nonhydrostatic model is therefore used to study the applicability of HIRLAM's large-scale convection and condensation scheme on meso-γ-scales.

b. Sensitivity to the choice of the β parameter

Figure 3 shows the radar reflectivity frequency distributions produced by different configurations of the convection scheme, as described in Table 2. All configurations tend to overestimate the areas of both very strong (>32 dBZ) and very weak (<8 dBZ) reflectivity. Although the overestimation of weak echoes is in most of the cases noticeable, we focus on the strong echoes, because of their larger practical importance.

The model-produced frequency distributions seem to be very sensitive to the choice of the β parameter, especially with small grid spacing. NHH-2 tends to produce too strong echoes compared to NHH-1. However, NHH-2 simulates the amount of moderate reflectivities well, whereas NHH-1 mainly underestimates them.

Figure 4 shows the temporal evolution of the reflectivity skill score (frequency bias) with a threshold range of 0–70 dBZ. Such a threshold range mainly gives information about the areal coverage of the predicted rain. More details about the choice of the score are presented in the appendix.

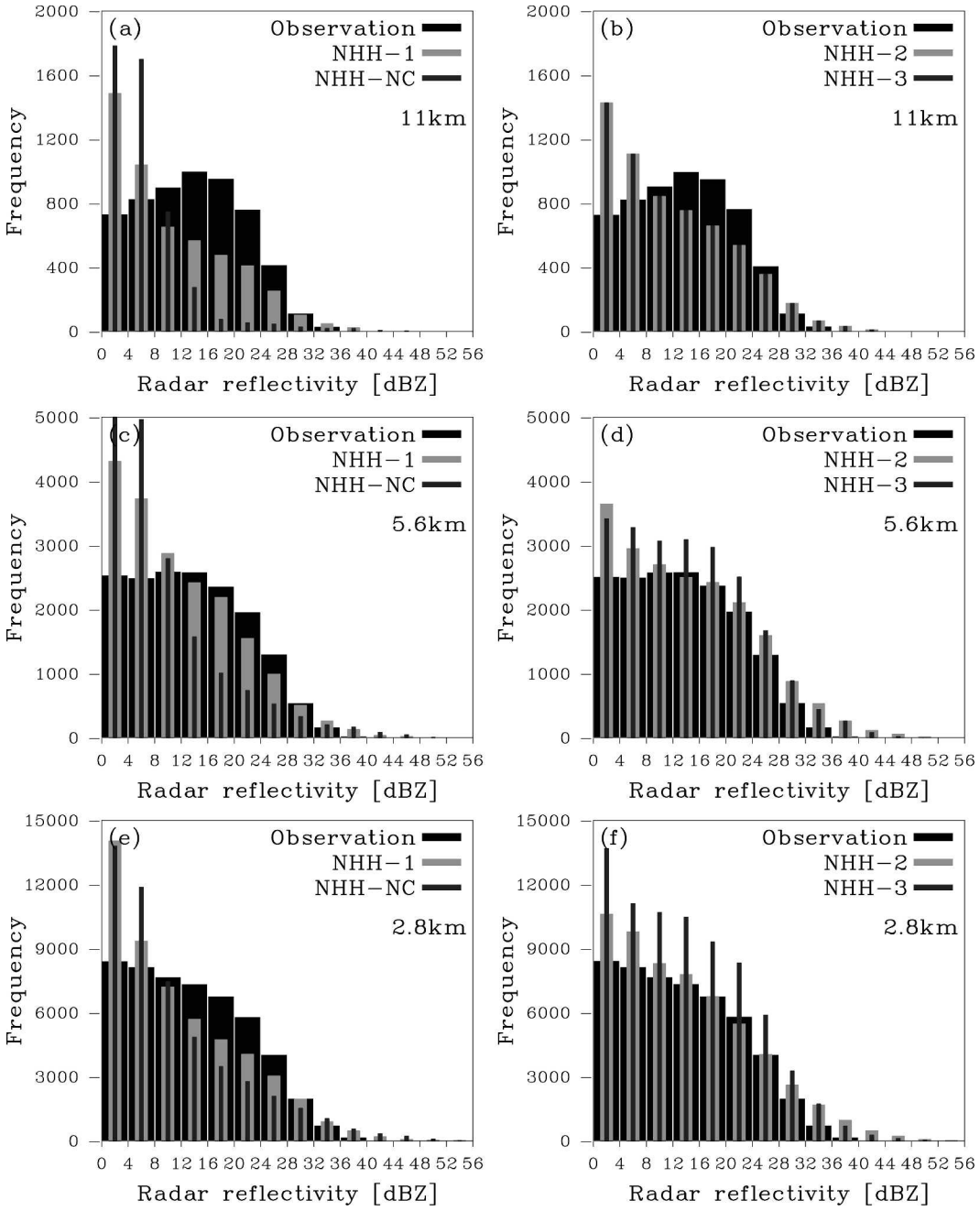

FIG. 3. Same as in Fig. 2, but the distributions are from (a), (c), (e) NHH-1 and NHH-NC and (b), (d), (f) NHH-2 and NHH-3.

In general, NHH-2 produces a better precipitation coverage compared to NHH-1 during the first 9 h of the simulation. NHH-2 (β depends on $\langle RH \rangle$) is able to simulate the extent of the precipitation area right from the beginning. However, during the most intense rain (hours 6–15) the best time series of frequency bias is produced by NHH-1 with a 5.6-km grid spacing. The remainder of the NHH-1 experiments (2.8 and 11 km) delays the onset of precipitation by 3–4 h.

Figure 5 presents 12-h accumulated areal precipitation as a function of grid spacing. Figures 5b,c show how the total precipitation is composed of the stratiform and convective parts of Eq. (17). NHH-1 produces average precipitation amounts that are close to the observed value provided by the Baltex Radar Data Center (Koistinen and Michelson 2002). It is evident that NHH-2 overestimates the areal precipitation at all grid spacings. Most of the precipitation, over 80%, origi-

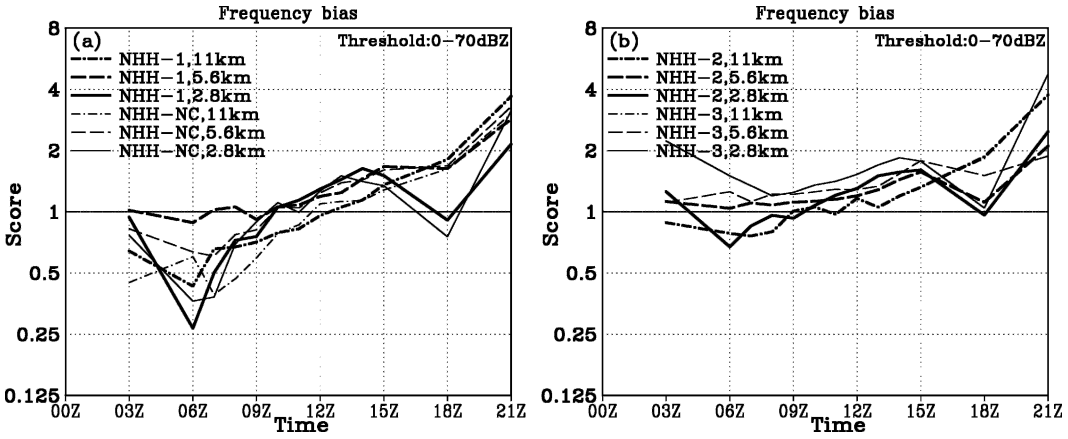

FIG. 4. Time series of reflectivity frequency bias: (a) NHH-1 (thick) and NHH-NC (thin); (b) NHH-2 (thick) and NHH-3 (thin). The dot–dash, dashed, and solid lines represent grid spacings of 11, 5.6, and 2.8 km, respectively. The radar antenna elevation is 0.4°.

nates from the convective part. In general, numerical models using a Kuo-type of convection parameterization tend to have a high proportion of convective rain (e.g., Wang and Seaman 1997).

To conclude, NHH-1 and NHH-2 react differently in the prevailing moist conditions (initially the difference between the temperature and the dewpoint temperature is less than 1°C in the layer between the 850-hPa

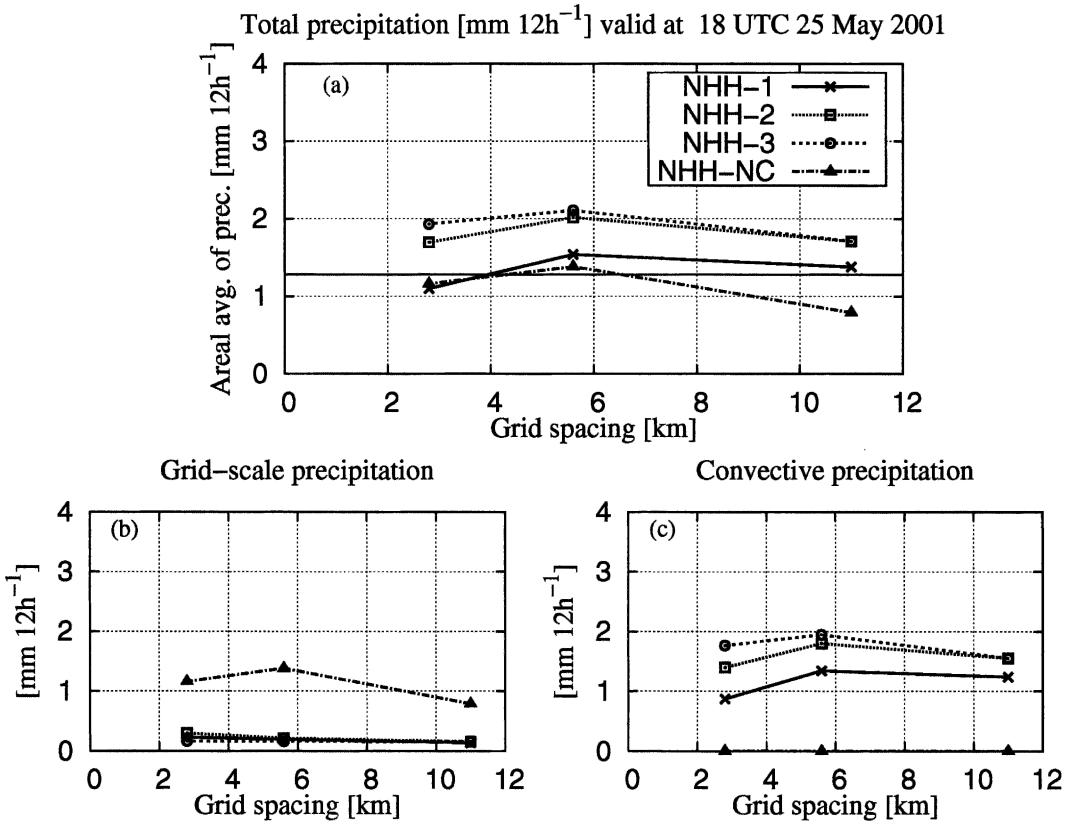

FIG. 5. Areally averaged 12-h accumulated precipitation as a function of the grid spacing: (a) total precipitation, (b) grid-scale precipitation, and (c) convective precipitation. Areal averages are defined over the area shown in Fig. 1. The solid horizontal line in (a) represents an areally averaged radar retrieval of accumulated precipitation provided by the Baltex Radar Data Center.

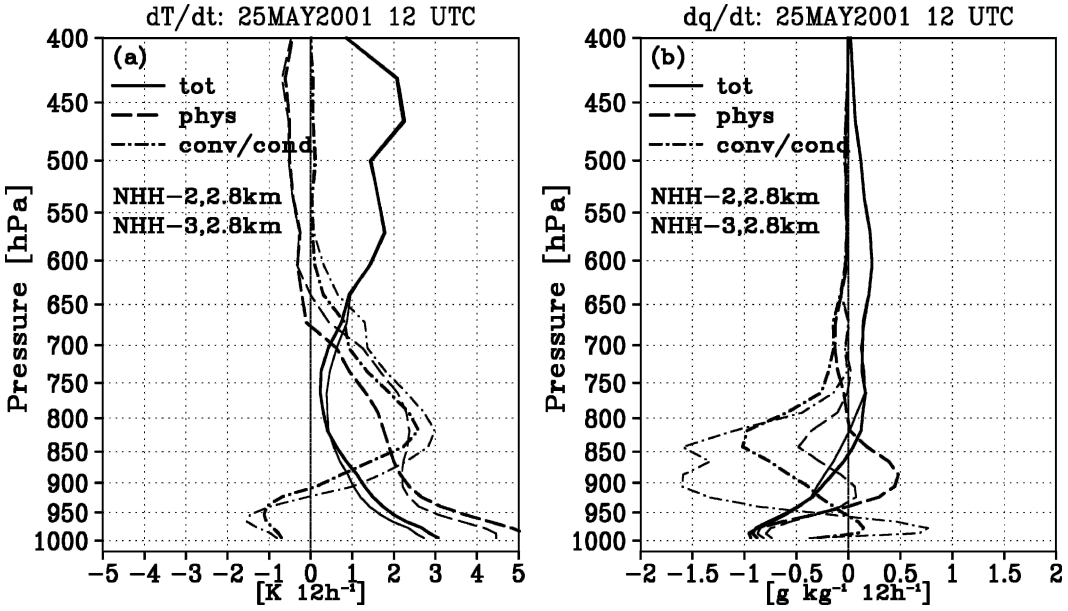

FIG. 6. Areally averaged 12-h tendencies of (a) temperature [K (12 h)$^{-1}$] and (b) specific humidity [g kg^{-1} (12 h)$^{-1}$]. Solid lines represent total tendency (physics + dynamics), dashed lines represent tendency due to model physics (radiation, turbulence, convection, and condensation), and dash–dot lines represent tendency due to condensation and convection processes. Thick curves are from NHH-2 while thin ones are from NHH-3. The horizontal grid spacing is 2.8 km.

pressure level and the surface). As Eq. (15) states, the convection scheme of NHH-2 mainly distributes the moisture input into heating and cloud condensate in moist conditions. In NHH-1, the larger proportion of the moisture input is used to moisten the convective air column [Eq. (16)]. Consequently, NHH-2 produces more precipitation and stronger reflectivities compared to NHH-1 [see Eq. (17)].

c. *The effect of the grid-size-dependent triggering mechanism*

The grid-size-dependent triggering mechanism for convection [Eqs. (1)–(5)] is clearly beneficial at higher model resolutions (Figs. 3d,f) as can be seen by comparing NHH-2 and NHH-3. NHH-3 increasingly overestimates the amount of moderate reflectivities as the grid spacing decreases. Evidently, without any dependency on model resolution the convection scheme is too active. This will also lead to slightly too wide precipitation areas, with weak reflectivities, as can be seen from Fig. 1d. However, the grid-size-dependent triggering mechanism does not have an effect on strong reflectivities. Both NHH-2 and NHH-3 overestimate the areas of strong echoes.

The temporal evolution of the frequency bias indexes of NHH-2 and NHH-3 is shown in Fig. 4b. NHH-3 overestimates the extent of the precipitation coverage, whereas NHH-2 performs better. The difference is most noticeable during the first 9 h of the simulation, especially with a high model resolution.

The effect of the grid-size dependency on 12-h accumulated precipitation is shown in Fig. 5. Both NHH-2 and NHH-3 overestimate the average precipitation amount for reasons explained in section 4b. However, in NHH-2 the amount of convective precipitation is decreased compared to NHH-3 as the grid spacing is reduced. This effect starts to be significant with a smaller grid spacing than 3 km. Consequently, the proportion of the grid-scale precipitation increases and the convective precipitation decreases. Similar behavior is obtained in other numerical simulations (e.g., Lean and Clark 2003). NHH-3 keeps the ratio between grid-scale and convective precipitation nearly constant.

Figure 6 shows temperature and specific humidity tendency profiles produced by NHH-2 and NHH-3 with a 2.8-km grid spacing. The magnitude of heating in the 900–600-hPa layer and cooling near the surface due to convection and condensation is smaller in NHH-2 compared to NHH-3. Furthermore, NHH-2 dries the air layer between 950–750 hPa less than NHH-3 does. The tendency profiles of both NHH-2 and NHH-3 with 5.6- and 11-km grid spacings closely follow the profiles of NHH-3 with a 2.8-km grid (not shown for clarity).

The results for NHH-2 are in line with Jung and

Arakawa (2004), who showed that the required tendencies due to cloud microphysics are weaker at higher model resolutions. Here the tendencies due to convection and condensation are reduced by introducing the grid-size-dependent triggering mechanism. However, this approach is only active with a smaller grid spacing than 10 km and becomes truly effective with a grid spacing of less than 3 km.

The modifications in the convection scheme have a strong influence on the combined tendencies of the physical processes. However, the dynamical processes efficiently compensate the differences due to the physics, resulting in only a small difference in total tendency. It should be emphasized that the difference between the tendencies due to the convection and condensation processes cannot solely explain the difference in the physics tendencies. Even if the source of the tendency difference is the convection scheme, there are also other contributors, such as turbulence and radiation, which naturally react to the changing conditions produced by the convection scheme. For clarity, those processes are not presented individually in Fig. 6.

d. The comparison between explicit and parameterized convection

The experiment without a convection scheme (NHH-NC) significantly underestimates the amount of moderate reflectivities (Fig. 3). NHH-NC also overestimates the frequency of strong reflectivities. Nevertheless, this overestimation is not as severe as for NHH-2 and NHH-3. As the grid spacing diminishes, the frequency distribution of NHH-NC approaches the observed one. However, even with a 2.8-km grid spacing, the distribution without convection parameterization is worse than for those with the full physics.

The time series of the frequency bias index (Fig. 4) indicate that, without convection parameterization, the onset of precipitation is delayed more than with the full physics (i.e., NHH-1 and NHH-2). As expected, this feature is more evident with a coarse grid. Although the coverage of rain areas of NHH-NC are similar to those of NHH-1 and NHH-2 with a 2.8-km grid spacing (Figs. 1a,c,e), NHH-NC reaches strong dBZ values later than the other experiments (not shown). If convective condensation is not allowed, the formation of precipitation is only based on the production of cloud condensate in the stratiform regime [via Eq. (17)]. The time scale for producing the precipitation is larger in the stratiform than in the convective regime, as shown by Eq. (18). For this reason, NHH-NC delays the formation of precipitation more than those with the full physics. Moreover, without the subgrid condensation of the convection scheme the rain intensity will also be too strong.

NHH-NC with an 11-km grid size clearly underestimates the average precipitation amount (Fig. 5a). The results approach the observed value as the grid spacing decreases. However, it should be emphasized that the well-represented average precipitation amount is a consequence of the poorly represented reflectivity distribution, as discussed above.

5. Conclusions

Model simulations of a single cold air outbreak event with convective precipitation over southern Finland (25 May 2001) have been conducted in order to investigate the applicability of the HIRLAM's convection and condensation scheme on the meso-γ-scales. The performance of the nonhydrostatic version of HIRLAM in moist convective conditions has also been studied. Model results are validated against radar reflectivity data using an external postprocessor that calculates radar reflectivities from the model-produced precipitation field.

The issue of model comparison in different atmospheric conditions is not new. From the meteorological point of view, such studies have usually concentrated on extreme events [e.g., frontal precipitation and mesoscale convective systems by Wang and Seaman (1997); squall lines by Bélair and Mailhot (2001)]. However, weakly forced shallow convection conditions are also important for operational NWP purposes. In particular, the meteorological conditions presented in this paper are common in Finland during spring and early summer.

From the modeling point of view, Kuo-type convection schemes have not been widely studied at meso-γ-scales mainly due to their poor performance even at scales of 10–40 km (e.g., Wang and Seaman 1997). The physical justification of the Kuo scheme has also been criticized (e.g., Raymond and Emanuel 1993). However, the convection parameterization in HIRLAM (part of the STRACO scheme) differs considerably from the original Kuo scheme. The cumulus parameterization used in STRACO does not directly produce any precipitation. However, the precipitation release depends on prognostic cloud condensate. Contrary to the Kuo scheme, STRACO also includes the cooling effect of the evaporating precipitation below the cloud base. The normalized convective heating and moistening profiles, which are used in our case, are regarded to be more realistic than the ones in the original Kuo scheme (Raymond and Emanuel 1993). The STRACO scheme has been successfully employed in the operational NWP with grid spacings of 10–50 km over a decade.

The best results are obtained with nonhydrostatic dynamics, with a fully grid-size-dependent convection scheme (i.e., triggering mechanism and moistening parameter) and with a 5.6-km grid spacing. This combination produces a reflectivity distribution that resembles the observed one surprisingly well. The time evolution of the precipitation area, especially during the first half of the simulation, also outperforms the results from the other combinations. Nevertheless, a slight overestimation of the strong reflectivity value amount is present.

None of the convection schemes employed for a 2.8-km grid spacing is able to produce satisfactory results. Nevertheless, the experiments with a grid-size-dependent moistening parameter for convection parameterization produce reflectivity distributions and average precipitation amounts that most resemble the observations. However, the onset of convective precipitation is delayed by 3–4 h with all grid spacings except 5.6 km. This indicates that the moistening parameter, which depends only on the grid size, is too simplified and case dependent to provide a satisfactory solution for all scales between 2.8 and 11 km. The ⟨RH⟩-dependent moistening parameter for the convection scheme is able to help the model to predict the onset of precipitation more precisely. However, this approach overestimates the average precipitation amount at all the scales considered by creating far too strong radar reflectivities (i.e., rain intensity).

The grid-size-dependent triggering mechanism for convection parameterization is evidently beneficial for models operating with a dense grid. This approach reduces the overestimation of the average precipitation by deactivating the convective heating and condensation as the grid spacing decreases. However, the triggering mechanism employed in the present study becomes really effective with grid spacings smaller than 3 km.

In the simulations with an explicit treatment of convection, the onset of precipitation is delayed more than with the full physics. Similar behavior has been seen in several studies (e.g., Zhang et al. 1988; Wang and Seaman 1997; Liu et al. 2001). The results of the explicit simulation approach the observations as the grid spacing decreases. However, for all scales considered, the performance of the simulations without convection parameterization is worse than with the full physics.

The nonhydrostatic model outperforms the hydrostatic model in the present moist convective case at the 5.6- and 2.8-km horizontal grid spacings. The hydrostatic model is not able to produce the cellular features of the observed event. It also overestimates (underestimates) the amount of strong (moderate) reflectivities. With an 11-km grid spacing, both models perform equally well.

A limitation of the present study is that the simulations are conducted for a single case only. Although the convective conditions studied here are typical of those in Finland, future studies should be extended to a larger variety of atmospheric phenomena. More interest should be directed in particular into severe thunderstorm activity with extreme precipitation. Dynamically forced conditions, such as squall lines created by frontal systems, also need to be studied. In addition, the version of the HIRLAM convection and condensation scheme tested here should be validated in parallel with more sophisticated microphysical schemes that have prognostic variables for different hydrometeors. These issues, however, were beyond the scope of the present study.

Acknowledgments. We thank Rein Rõõm and Aarne Männik for providing valuable help in the use of the nonhydrostatic dynamical package, and Bent Hansen Sass for providing the experimental version of the STRACO scheme and for useful comments during the work. We thank also an anonymous reviewer whose comprehensive comments helped to improve the original manuscript significantly.

APPENDIX

Skill Scores

Skill scores are the main tools for verification of NWP precipitation forecasts. Skill scores give information about the spatial accuracy of a predicted precipitation area. The intensity of the rain can be evaluated by using threshold values for the desired quantity (e.g., accumulated precipitation or radar reflectivity). For example, a large threshold (e.g., 5 mm h^{-1}) should be used when verifying strong precipitation events. By contrast, a small threshold is needed in a verification of the horizontal extent of the precipitation. There are several different scores, whose usefulness depends on the case. Wilson (2001) has given a review of available skill scores, concentrating on their strengths and weaknesses.

The determination of skill scores is based on a contingency table (A, B, C, D), in which A represents the number of grid points with a successful prediction, B is the number of grid points where the event is predicted but not observed, C is the number of grid points where the event is observed but not predicted, and D is the number of grid points where the event is neither predicted nor observed.

In the present study, we have used only the frequency bias index (FBI). FBI gives the ratio between the total number of points with forecast occurrence and those with observed occurrence:

$$\mathrm{FBI} = \frac{A + B}{A + C}. \tag{A1}$$

The perfect score is 1. FBI is very useful for studying the coverage of the predicted precipitation area.

REFERENCES

Anthes, R. A., 1977: A cumulus parameterization scheme utilizing a one-dimensional cloud model. *Mon. Wea. Rev.,* **105,** 270–286.

Arakawa, A., 2004: The cumulus parameterization problem: Past, present, and future. *J. Climate,* **17,** 2493–2525.

Bélair, S., and J. Mailhot, 2001: Impact of horizontal resolution on the numerical simulation of a midlatitude squall line: Implicit versus explicit condensation. *Mon. Wea. Rev.,* **129,** 2362–2376.

Braham, R., 1952: The water and energy budgets of the thunderstorm and their relation to thunderstorm development. *J. Meteor.,* **9,** 227–242.

Chamberlain, C. A., 1953: Aspects of travel and deposition of aerosol and vapour clouds. Tech. Rep. R-1261, A.E.R.E. Harwell, United Kingdom, 30 pp.

Cohen, C., 2000: A quantitative investigation of entrainment and detrainment in numerically simulated cumulonimbus clouds. *J. Atmos. Sci.,* **57,** 1657–1674.

Cuxart, J., P. Bougeault, and J.-L. Redelsperger, 2000: A turbulence scheme allowing for mesoscale and large-eddy simulations. *Quart. J. Roy. Meteor. Soc.,* **126,** 1–30.

Haase, G., and S. Crewell, 2000: Simulation of radar reflectivities using a mesoscale weather forecast model. *Water Resour. Res.,* **36,** 2221–2231.

——, and C. Fortelius, 2001: Simulation of radar reflectivities using HIRLAM forecasts. HIRLAM Tech. Rep. 51, SMHI, Norrköping, Sweden, HIRLAM-5 Project, 22 pp. [Available online at http://hirlam.knmi.nl/open/publications/TechReports/.]

Hammarstrand, U., 1998: Questions involving the use of traditional convection parameterization in NWP models with higher resolution. *Tellus,* **50A,** 265–282.

Jung, J.-H., and A. Arakawa, 2004: The resolution dependence of model physics: Illustrations from nonhydrostatic model experiments. *J. Atmos. Sci.,* **61,** 88–102.

Kato, T., and K. Saito, 1995: Hydrostatic and non-hydrostatic simulations of moist convection: Applicability of the hydrostatic approximation to a high-resolution model. *J. Meteor. Soc. Japan,* **73,** 59–77.

Koistinen, J., and D. B. Michelson, 2002: Baltex weather radar-based products and their accuracies. *Boreal Environ. Res.,* **7,** 253–263.

Kuo, H. L., 1974: Further studies of parameterization of the influence of cumulus convection on large-scale flow. *J. Atmos. Sci.,* **31,** 1232–1240.

Lean, H. W., and P. A. Clark, 2003: The effects of changing resolution on mesoscale modelling of line convection and slantwise circulations in FASTEX IOP16. *Quart. J. Roy. Meteor. Soc.,* **129,** 2255–2278.

Liu, C., M. W. Moncrieff, and W. W. Grabowski, 2001: Hierarchial modelling of tropical convective systems using explicit and parameterized approaches. *Quart. J. Roy. Meteor. Soc.,* **127,** 493–515.

Männik, A., and R. Rõõm, 2001: Nonhydrostatic adiabatic kernel for HIRLAM. Part II: Anelastic, hybrid-coordinate, explicit-Eulerian model. HIRLAM Tech. Rep. 49, SMHI, Norrköping, Sweden, HIRLAM-5 Project, 51 pp. [Available online at http://hirlam.knmi.nl/open/publications/TechReports/.]

——, ——, and A. Luhamaa, 2003: Nonhydrostatic generalization of a pressure-coordinate-based hydrostatic model with implementation in HIRLAM: Validation of adiabatic core. *Tellus,* **55A,** 219–231.

Molinari, J., and M. Dudek, 1992: Parameterization of convective precipitation in mesoscale models: A critical review. *Mon. Wea. Rev.,* **120,** 326–344.

Montanari, A., and S. Uhlenbrook, 2004: Catchment modelling: Towards an improved representation of the hydrological processes in real-world model applications. *J. Hydrol.,* **291,** 159.

Noilhan, J., and S. Planton, 1989: A simple parameterization of land surface processes for meteorological models. *Mon. Wea. Rev.,* **117,** 536–549.

Orlanski, I., 1975: A rational subdivision of scales for atmospheric processes. *Bull. Amer. Meteor. Soc.,* **56,** 527–530.

Raymond, D. J., and K. A. Emanuel, 1993: The Kuo cumulus parameterization. *The Representation of Cumulus Convection in Numerical Models, Meteor. Monogr.,* No. 46, Amer. Meteor. Soc., 145–147.

Rõõm, R., 2001: Nonhydrostatic adiabatic kernel for HIRLAM. Part I: Fundamentals of nonhydrostatic dynamics in pressure-related coordinates. HIRLAM Tech. Rep. 48, SMHI, Norrköping, Sweden, HIRLAM-5 Project, 25 pp. [Available online at http://hirlam.knmi.nl/open/publications/TechReports/.]

Sass, B. H., 2002: A research version of the STRACO cloud scheme. DMI Tech. Rep. 02-10, Danish Meteorological Institute, Copenhagen, Denmark, 25 pp. [Available online at http://www.dmi.dk/dmi/index/viden/dmi-publikationer/tekniskerapporter.htm.]

Savijärvi, H., 1990: Fast radiation parameterization schemes for mesoscale and short-range forecast models. *J. Appl. Meteor.,* **29,** 437–447.

Sundqvist, H., 1993: Inclusion of ice phase of hydrometeors in cloud parameterization for mesoscale and largescale models. *Contrib. Atmos. Phys.,* **66,** 137–147.

——, E. Berge, and J. E. Kristjánsson, 1989: Condensation and cloud parameterization studies with a mesoscale numerical weather prediction model. *Mon. Wea. Rev.,* **117,** 1641–1657.

Tao, W.-K., D. Starr, A. Hou, P. Newman, and Y. Sud, 2003: A cumulus parameterization workshop. *Bull. Amer. Meteor. Soc.,* **84,** 1055–1062.

Uhlenbrook, S., S. Roser, and N. Tilch, 2004: Hydrological process representation at the meso-scale: The potential of a distributed, conceptual catchment model. *J. Hydrol.,* **291,** 278–296.

Undén, P., and Coauthors, 2002: HIRLAM-5 scientific documentation. HIRLAM-5 project, SMHI, Norrköping, Sweden, 144

pp. [Available online at http://hirlam.knmi.nl/open/publications/SciDoc_Dec2002.pdf.]

Wang, W., and N. L. Seaman, 1997: A comparison study of convective parameterization schemes in a mesoscale model. *Mon. Wea. Rev.,* **125,** 252–278.

Weisman, M. L., W. C. Skamarock, and J. B. Klemp, 1997: The resolution dependence of explicitly modeled convective systems. *Mon. Wea. Rev.,* **125,** 527–548.

Wilson, C., 2001: Review of current methods and tools for verification of numerical forecasts of precipitation. Met Office, United Kingdom, COST 717 Working Document WDF-02-200109-1, 14 pp. [Available online at http://pub.smhi.se/cost717/.]

Zhang, D. L., E. Y. Hsie, and M. W. Moncrieff, 1988: A comparison of explicit and implicit predictions of convective and stratiform precipitating weather systems with a meso-β scale numerical model. *Quart. J. Roy. Meteor. Soc.,* **114,** 31–60.